Astronomy & Astrophysics manuscript no. 4u1636_11_VII
July 19, 2016

Long-term quasi-periodicity of 4U 1636–536 resulting from accretion disc instability

Mateusz Wiśniewicz[1], Dorota Gondek-Rosińska[1], Agnieszka Słowikowska[1], Andrzej A. Zdziarski[2], and Agnieszka Janiuk[3]

[1] Janusz Gil Institute of Astronomy, University of Zielona Góra, Szafrana 2, PL-65-516 Zielona Góra, Poland
e-mail: mateusz@astro.ia.uz.zgora.pl
[2] Centrum Astronomiczne im. M. Kopernika, Bartycka 18, PL-00-716 Warszawa, Poland
[3] Centre for Theoretical Physics, Polish Academy of Sciences, Al. Lotników 32/46, PL-02-668 Warsaw, Poland

July 19, 2016

ABSTRACT

We present the results of a study of the low-mass X-ray binary 4U 1636–536. We have performed temporal analysis of all available *RXTE*/ASM, *RXTE*/PCA, *Swift*/BAT and MAXI data. We have confirmed the previously discovered quasi-periodicity of $\simeq 45$ d present during ∼2004, and we have found it continued to 2006. At other epochs, the quasi-periodicity is only transient, and the quasi-period, if present, drifts. We have then applied a time-dependent accretion disc model to the interval with the significant X-ray quasi-periodicity. Although 4U 1636–536 is persistent, the observed quasi-periodicity can be well modelled by the hydrogen thermal-ionization instability occurring in outer regions of the accretion disc. For our best model, the period and the amplitude of the theoretical light curve agree well with those observed. The model parameters are the average mass accretion rate (estimated from the light curves), and the accretion disc viscosity parameters, $\alpha_{\rm cold}$ and $\alpha_{\rm hot}$, for the hot and cold phases, respectively. Our best model gives relatively low values of $\alpha_{\rm cold} \simeq 0.01$ and $\alpha_{\rm hot} \simeq 0.03$.

Key words. accretion, accretion discs – instabilities – stars: individual: (4U 1636–536, V801 Ara) – X-rays: binaries

1. Introduction

4U 1636–536 is a low-mass X-ray binary (LMXB) discovered by Willmore et al. (1974). The photometry of the optical counterpart (V801 Ara) shows a short orbital period of 3.79 h (Giles et al. 2002). The binary system consists of a late-type, low-mass ($\simeq$ 0.3–0.4 $M_\odot$) donor, which transfers mass onto a neutron star (Fujimoto & Taam 1986; van Paradijs et al. 1990). Galloway et al. (2006) estimated the distance to 4U 1636–536 to be $D = 6.0 \pm 0.5$ kpc from Eddington limited X-ray bursts, assuming the neutron star mass of 1.4 $M_\odot$ and the stellar radius of 10 km. According to Casares et al. (2006), the mass function and mass ratio of 4U 1636–536 are $f(M) = 0.76 \pm 0.47\,M_\odot$ and $M_2/M_{\rm NS} \simeq 0.21$–$0.34$, respectively, where $M_{\rm NS}$ is the mass of the neutron star and M_2 is the mass of the donor. They also estimated the inclination angle as $i \simeq 36°$–$60°$. The binary is a persistent X-ray source, although it shows significant flux variations on both long and short time scales. On time scales of hours, its flux varies by a factor of ∼2–3 (Hoffman et al. 1977; Ohashi et al. 1982; Breedon et al. 1986; Hasinger & van der Klis 1989). The presence of kHz quasi-periodic oscillations, which are also visible in the system during X-ray bursts, shows that the neutron star has been spun-up through accretion (Zhang et al. 1996; Strohmayer 1999).

4U 1636–536 has been monitored daily in the 1.3–12.2 keV energy range by the All Sky Monitor (ASM) on-board of the *Rossi X-ray Timing Explorer* (*RXTE*) from 1996 until 2011. During the first four years of *RXTE*/ASM observations (1996–2000) the source count rate was relatively stable at ~ 15 cts s^{-1}, see the upper panel of Fig. 1. After 2000, it started to gradually decline and occasionally show a statistically significant quasi-periodic variability (Shih et al. 2005). Those authors reported the presence of a long-period, $\simeq 47$ d, quasi-periodic variability in the 2004 light curve. They suggested that the observed flux variability is caused by the variability of the accretion flow related to X-ray irradiation of the disc. From March 2005 to September 2006, Belloni et al. (2007) performed *RXTE*/PCA monitoring campaign of 4U 1636–536, finding the light curves to display

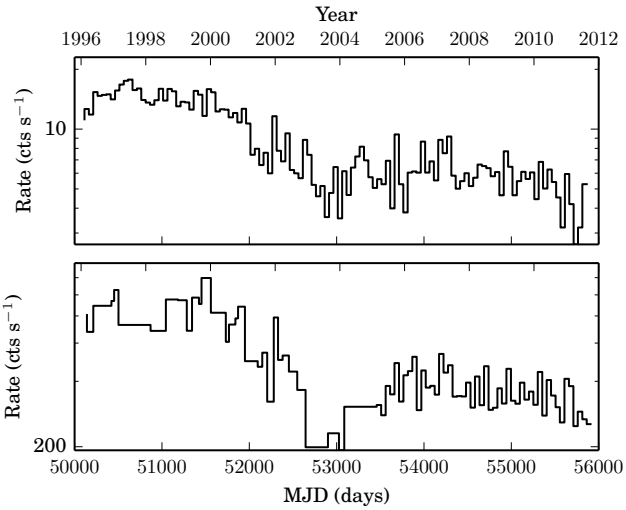

Fig. 1. Top: The 50-d average *RXTE*/ASM light curve of 4U 1636–536 in the energy range of 1.3–12.2 keV from January 1996 to November 2011. Bottom: The 50-d average *RXTE*/PCA light curve in the energy range of 2–60 keV for the same range of time.

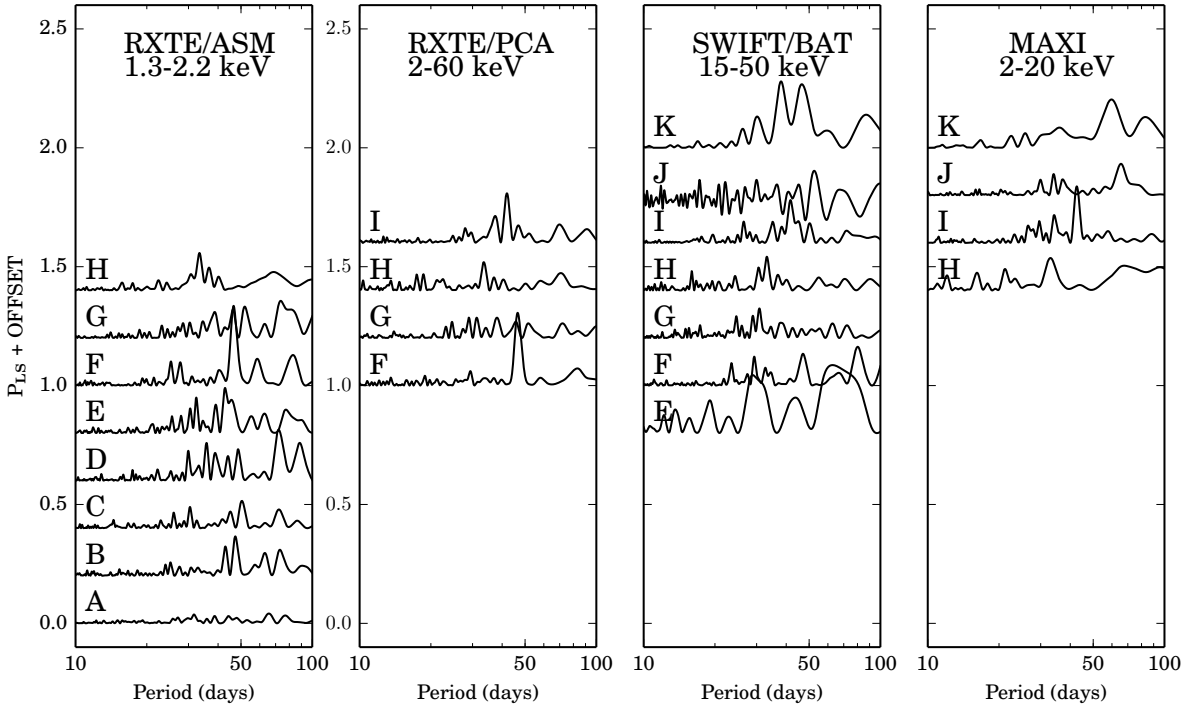

Fig. 2. The power spectra (with offsets) for the *RXTE*/ASM (first panel), the *RXTE*/PCA (second panel), the *Swift*/BAT (third panel) and the MAXI (fourth panel) in the time intervals given in MJD by: (A) 50088–50741, (B) 50742–51452, (C) 51453–52162, (D) 52163–52886, (E) 52887–53564, (F) 53565–54185, (G) 54186–54749, (H) 54750–55322, (I) 55323–55869, (J) 55893–56461, (K) 56462–56738.

30–40 d quasi-periodic variability. In 2008, Shih et al. (2011) conducted a 3–month observational campaign of 4U 1636–536 in the optical and X-ray bands using the NOAO SMART telescope, *RXTE*/ASM and *Swift*/BAT. They showed that optical time-scale variability is correlated with the soft X-ray modulation. They also analysed *RXTE*/ASM and *Swift*/BAT archival data from 2005 to 2009 and confirmed the presence of quasi-periodic variability of 4U 1636–536 after Shih et al. (2005). Then, Farrell et al. (2009) confirmed the anticorrelation between soft and hard X-ray light curve in 4U 1636–536. They analysed data from *Swift*/BAT and *RXTE*/ASM and reported 46–d quasi-periodic variability.

In our paper, we study the variability of 4U 1636–536 taking into account the currently available data from four X-ray detectors, spanning almost 20 years (1996–2014). We interpret the data in terms of a disc instability model. In Sect. 2, we describe the X-ray data and perform their timing analysis. In Sect. 3, we present the theoretical model of evolution of an accretion disc around a neutron star used in the paper. We model the evolution of the accretion disc for a wide range of viscosity parameters. We find that the observed quasi-periodicity can be explained by the thermal instability due to the ionisation of hydrogen. We discuss our results, and finally, in Sect. 4, we give our main conclusions.

2. Data analysis

We analyse the X-ray data obtained with the *RXTE*/ASM (Bradt et al. 1993; Levine et al. 1996), the *RXTE*/PCA (Jahoda et al. 1996), the Burst Alert Telescope (BAT) on board of *Swift* (Markwardt et al. 2005; Krimm et al. 2013) and the Monitor of All-sky X-ray Image (MAXI) on board of *International Space Station* (Matsuoka et al. 2009). One-day average data from these instruments have been used to analyse the flux variability at different epochs. The ASM operated in the energy range of 1.3–12.2 keV with the sensitivity of $\sim$ 30 mCrab, while the PCA operated in the energy range of 2–60 keV with the sensitivity of 0.1 mCrab. The BAT observes 88% of the sky each day with the sensitivity of $\sim$ 5 mCrab in the energy range of 15–50 keV. It has observed 4U 1636–536 since 2005. The Japanese X-ray camera MAXI has observed X-ray sources since August 2009, scanning most of the sky every 96 minutes. It operates in the energy range of 2–20 keV with the sensitivity of 20 mCrab.

The X-ray flux history in the ASM and the PCA data are shown in Fig. 1. The light curves can be divided into three main parts. Focusing on the ASM data, we see that the flux was relatively stable ($\sim$ 15 cts s^{-1}) from 1996 to 2000, with only some low-amplitude variability. Between 2000 and 2003, the flux gradually declined to a level below $\sim$ 10 cts s^{-1} and stayed below this level in the later epochs. In the case of the PCA data, it can be seen that the decline of the flux was until 2004.

We have linearly detrended all the data and then applied a Fourier transform. We use the standard Lomb-Scargle method (Scargle 1982), as implemented in the astroML (VanderPlas et al. 2012) Python library. This method is suitable for our unevenly sampled time series. We have used a bootstrap method to compute Lomb-Scargle significance levels (Ivezić et al. 2014). We have divided all the data into 11 intervals with the length of $\simeq$ 2 yr each, denoting them with the capital letters: A: 1996–1997, B: 1997–1999, C: 1999–2001, D: 2001–2003, E: 2003–2005, F: 2005–2007, G: 2007–2008, H: 2008–2010, I: 2010-2011, J: 2011-2013, and K: 2013-2014. The power spectra of

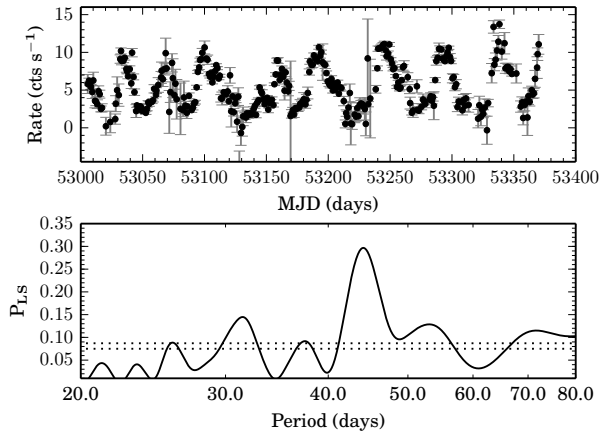

Fig. 3. Top: one-day average *RXTE*/ASM light curve for 2004. Bottom: the corresponding power spectrum. The dotted lines show the 99% and 95% significance levels determined by 1000 bootstrap resampling.

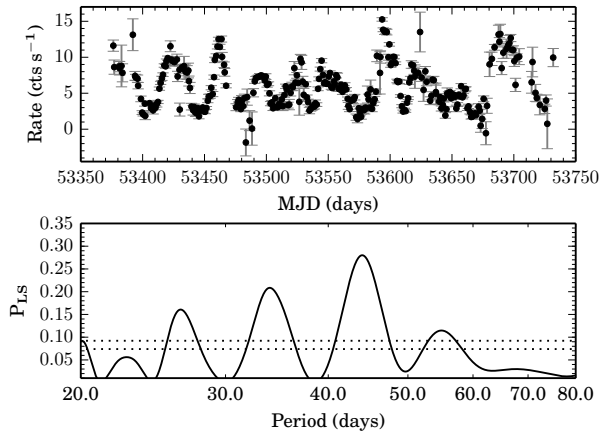

Fig. 4. The same as in Fig. 3 but for 2005.

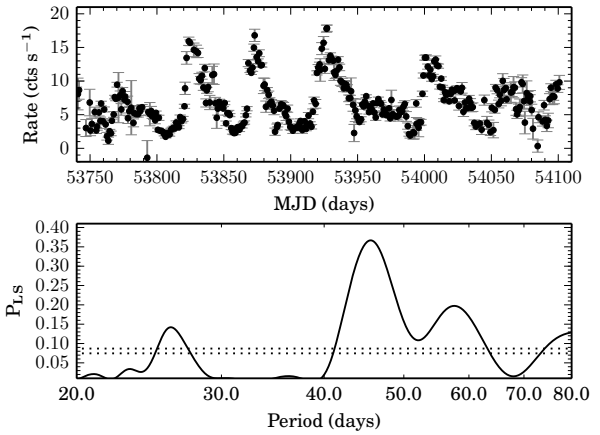

Fig. 5. The same as in Fig. 3 but for 2006.

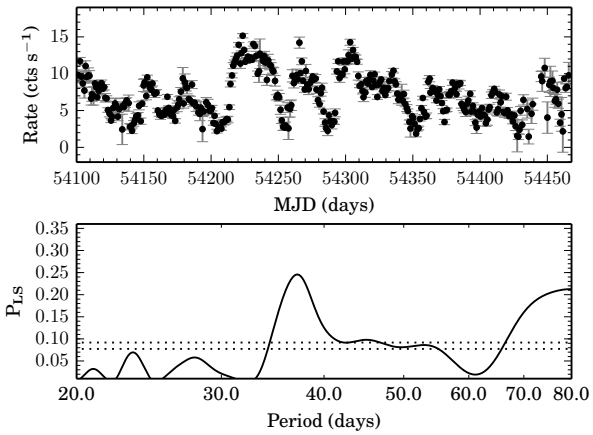

Fig. 6. The same as in Fig. 3 but for 2007.

these intervals for the data obtained with four instruments are shown in Fig. 2.

We then focus on 2-yr intervals from the ASM data shown in the Fig. 2. We see no periodicity in the interval A. From B to D, some quasi-periodicity appears, but is not statistically significant, with the peaks in the power spectra being low. Finally, from the interval E (2003–2005), significant quasi-periodicity is visible. A similar periodicity was noticed by Shih et al. (2005) for the 2004 epoch. The quasi-periodic variability began to gradually decline from the interval G.

In order to perform a more detailed analysis, for the time span where significant quasi-periodicity is visible, we focus on the power spectra of the ASM data from the second half of the interval E, whole interval F, and to the first half of the interval G, i.e. 2004–2007. Therefore, for this time span the data were divided into 1-yr intervals. The light curves and the corresponding power spectra are shown in Figs. 3–6. Relatively strong quasi-periodic variability is visible in 2004, 2005 and 2006, where the power spectra maxima are at $P = 44.5$ d, 44.0 d and 45.5 d, respectively. In 2007, the Lomb-Scargle power significantly decreased to $P_{\rm LS} \sim 0.25$ but also the power-spectrum maximum shifted to around 37 days, see Fig. 6. In the case of the *RXTE*/PCA, there were only relatively sparse data between 1996 to 2005, therefore we analysed only data after 2005, i.e. starting with the interval F. Again, there is a significant quasi-periodic signal with $P \simeq 45$ d, visible in the data of this interval, as well as in the interval I. In between, i.e. for the intervals G and H, only insignificant quasi-periodicities appear.

The BAT data are relatively noisy. We see some quasi-periodicity with $P \simeq 45$ d in the interval F. Then, it seems that the period of the variability is decreasing until the interval I, where the 45-d periodicity is again visible.

In order to approximate the bolometric light curve of 4U 1636–536, the fluxes of the ASM and BAT in the Crab unit were summed. We show the individual light curves for soft and hard X-ray ranges and their sum in Fig. 7 for the time span of MJD 53755–53963 within the interval F. These are the most predominant periodic data in our whole sample and therefore this part of the light curve was later used as a template for our theoretical model. The *RXTE*/PCA data for the same time span are shown in the bottom panel of Fig. 7.

The apparent delay of the ASM light curve with respect to that of the BAT of about 10 d (calculated by cross-correlation) appears to be related to an anti-correlation between these bands reflecting the spectral softening from the hard spectral state to the soft one with the pivot energy of $\sim$ 10 keV (Farrell et al. 2009; Done et al. 2007). In an ideal case, the maximum of the flux above the pivot would be at the minimum flux below the

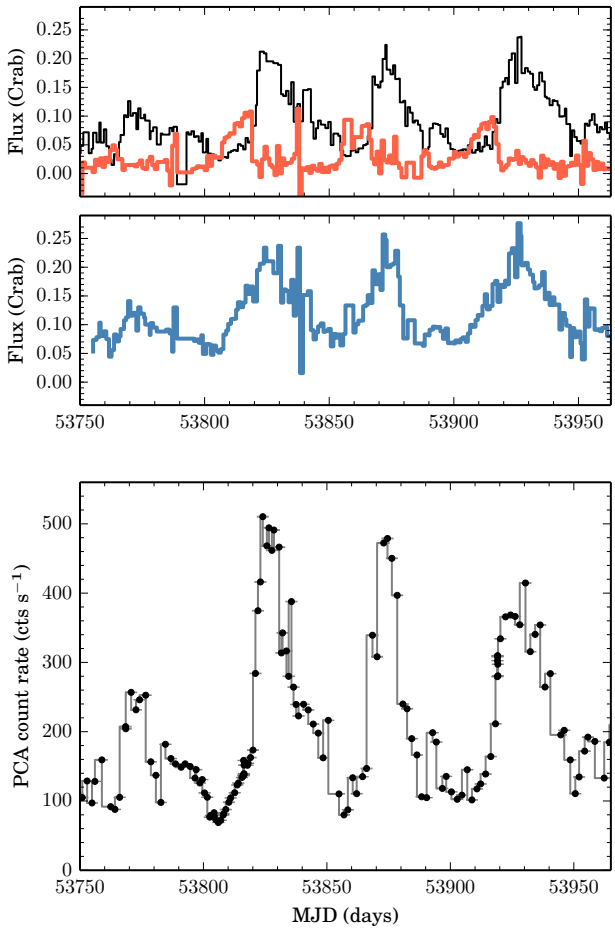

Fig. 7. Top: one-day average ASM 1.3–12.2 keV (thin black curve) and BAT 15–50 keV (thick red line) light curve of 4U 1636–536 from MJD 53755 to 53963 in Crab units. Middle: sum of one-day average ASM and BAT light curves (1.3–50 keV). Bottom: the 1-h averaged *RXTE*/PCA light curve for the same time interval.

pivot, which corresponds to the delay of a half of the period. In our case the pivot is within the ASM energy range, which then reduces the delay.

We see some ~40-d quasi-periodicity in the first 2-yr interval, H, of the MAXI data. In the next interval, I, there is a strong quasi-periodicity with $P \simeq 45$ d, similarly to the corresponding *Swift*/BAT data. Later, this periodicity disappears and another one with approximately doubled period, i.e. ≃70 d, appears.

3. The theoretical model

The theory of geometrically thin, stationary, accretion disc of Shakura & Sunyaev (1973) describes well accretion as the source of energy of many astrophysical objects. On the other hand, many of the observed accretion sources are strongly variable, which may be related to non-stationary effects predicted theoretically. In particular, Meyer & Meyer-Hofmeister (1982) and Smak (1982) independently found that accretion discs become unstable in the range of temperatures corresponding to ionization of hydrogen. This instability is the result of an inverse relation between the temperature and opacity in the range between $\sim 10^3$ K and $\sim 10^4$ K. The Rosseland mean opacity is smoothly decreasing with increasing temperature at higher temperatures. But when the temperature drops below 10^4 K, hydrogen partially recombines, and the opacity steeply decreases with decrease of temperature. Then, at $T \lesssim 10^3$ K, hydrogen becomes completely neutral, and the huge grain opacity dominates (Alexander 1975).

The theory of partial hydrogen ionisation instability was originally developed to explain the large-amplitude luminosity variations of cataclysmic variables (dwarf novae; Meyer & Meyer-Hofmeister 1982; Smak 1984). It is also believed that the same mechanism is responsible for outbursts in soft X-ray transients (Cannizzo et al. 1982; Dubus et al. 2001; Lasota 2001; Bagińska et al. 2014) and active galactic nuclei (Lin & Shields 1986; Clarke 1988; Mineshige & Shields 1990; Siemiginowska et al. 1996).

Also, Hameury et al. (1998) studied time dependent numerical models of accretion disc evolution to explain the cyclic outbursts of dwarf novae and soft X-ray transients. They used an adaptive grid technique, in which the outer radius of the disc, $R_{\rm out}$, is not fixed but it varies with time. In their simulations, the variable $R_{\rm out}$ allows for a propagation of the heat front from outer disc radii inwards, which is aimed to explain the properties of the dwarf nova SS Cygni.

Similarly, Dubus et al. (2001) used the adaptive grid numerical scheme. A large number of grid points, at least about 200–800, is required in such computations in order to conserve the mass of the disc, which was checked a posteriori by integration of the surface density over radius. Therefore, the numerical cell size used e.g., by Janiuk & Czerny (2007) was scaled with the disc height and fitted to the observations of X-ray binaries and AGN. In our computations, the outer disc radius is fixed, and the mass is conserved. We use a linear grid in $2\sqrt{r}$.

Then, King et al. (2004) showed that the magnetic dynamo process acting on local scales is able to produce only a small amplitude flickering. However, in order to reproduce the power-density spectra of the accreting NS (or BH) systems, the coherent magnetic alignment on larger spatial scales is required. Considering the findings of King et al. (2004), we keep the number of grid points at 300 to allow for moderate resolution. In this way, we assure that the thickness of the disc is not larger than the size of the disc cell, Δr, so the assumption of the geometrically thin disc is satisfied.

Lipunova & Shakura (2000, 2008) presented an analytical model of time dependent accretion disc, in which the continuity equation for the surface density change was solved. In this way, the authors explained the power-law decay of the luminosity and model the light curves of the X-ray novae. These authors do not compute numerically the thermal-viscous evolution and cyclic outbursts of the sources, because this would require solving the time-dependent thermal balance. Nevertheless, Suleimanov et al. (2008) successfully explained with such a model the decay profiles of the black-hole transients A 0620–00 and GX 1124–68. In our computations, we solve both the time-dependent evolution of the disc density and temperature; thus, modelling of cyclic outbursts and quiescent phases is possible.

We use the method of Smak (1984) in order to calculate the time evolution of an accretion disc around a neutron star. We follow the changes of the disc temperature and density. Then the surface temperature determines the emitted luminosity, observable in the X-ray band. We do not explicitly take into account the emission of the boundary layer, but include it in the estimate of the total luminosity as a function of the rate of mass supply at the disc outer radius.

3.1. Vertical structure of an accretion disc

In a geometrically thin accretion disc, the vertical and radial structures are decoupled (Pringle 1981). The equations that describe the disc vertical structure are very similar to those describing the internal structure of a star. For a Keplerian disc with the angular velocity, $\Omega = (GM/R^3)^{1/2}$, we have the energy balance,

$$\frac{\mathrm{d}F}{\mathrm{d}z} = -\alpha P \frac{\mathrm{d}\Omega}{\mathrm{d}R}, \tag{1}$$

where M is the mass of the accretor, F is the energy flux, α is the viscosity parameter, P is the pressure, and z and R are the height and radius of the accretion disc, respectively. Then, the hydrostatic equilibrium reads,

$$\frac{1}{\rho}\frac{\mathrm{d}P}{\mathrm{d}z} = -\Omega^2 z \equiv g_z, \tag{2}$$

where g_z is the vertical component of gravity. The energy transfer equation can be written as

$$\frac{\mathrm{d}\ln T}{\mathrm{d}z} = \frac{\mathrm{d}\ln P}{\mathrm{d}z}\nabla \tag{3}$$

where T, P and ρ are temperature, pressure and density, respectively, and $\nabla \equiv \mathrm{d}\ln T/\mathrm{d}\ln P$. In an optically-thick disc without convection, it is the radiative gradient,

$$\nabla = \nabla_{\rm rad} = \frac{\kappa P F}{4 P_{\rm rad} c g_z} \tag{4}$$

where κ is the Rosseland mean opacity and $P_{\rm rad}$ is the radiation pressure. However, in the case of partially ionized hydrogen, a major mode of energy transport may be due to convection, $\nabla_{\rm conv}$, which acts together with the radiative transport. We use here $\nabla = \nabla_{\rm conv} + \nabla_{\rm rad}$, where $\nabla_{\rm conv}$ is calculated using the mixing-length theory, as in stellar models (Paczyński 1969).

The equations are integrated between the disc midplane, $z = 0$, and the disc photosphere at the height H, given by the optical depth of the top layer of $\int_H^\infty \rho\kappa \mathrm{d}z = 2/3$, where ρ is the mass density (see Różańska et al. 1999). The tables of opacities are taken from Cox & Stewart (1969, 1970) and Seaton et al. (1994) for temperatures higher than $\log_{10} T > 3.5$ and from Alexander et al. (1983) for lower temperatures. At the photosphere, the effective temperature of the disc is $T_{\rm eff} = T(H)$, and $\sigma T_{\rm eff}^4 = Q^+ = Q^-$ is resulting from the heating of the disc through the viscous energy dissipation, Q^+, balanced by the radiative cooling, Q^-. The integration of equations for the vertical structure gives the surface density, $\Sigma = 2\int_0^H \rho \mathrm{d}z$.

The viscous energy dissipation rate per unit time and volume is $Q^+ = \frac{3}{2}\alpha P_{\rm tot}\Omega$, where we assumed that the viscous stress tensor R-ϕ component is proportional to the total pressure, and scaling with α (Shakura & Sunyaev 1973). Since we know the relation between the effective and central temperatures from the energy transfer equation, we can represent the energy balance in the Σ-$T_{\rm eff}$ diagram as a stability curve (Bath & Pringle 1982; Faulkner et al. 1983). The $T_{\rm eff}$ is directly related to the accretion rate, $\dot{M}$, which average is given by external conditions (i.e., the mass transfer rate from the companion star) and which is a parameter of the model. Example solutions are plotted in Fig. 8 for the accretor mass of $M_{\rm NS} = 1.4\ \mathrm{M}_\odot$ and selected values of the viscosity parameter, α, and the radius, R.

Calculating the time-dependent radial structure of an accretion disc can be significantly simplified because of the universality of the stability curve. The critical column densities, $\Sigma_{\rm min}$ and $\Sigma_{\rm max}$, between which its unstable branch appears (i.e. the points A and B in Fig. 8), are functions of the accretor mass (fixed in our case), the viscosity parameter, and the radius. On the other hand, the corresponding critical values of the effective temperature are given by the temperatures at which hydrogen becomes dominantly neutral or ionized, and thus are nearly universal, i.e., only weakly depend on the accretion flow parameters.

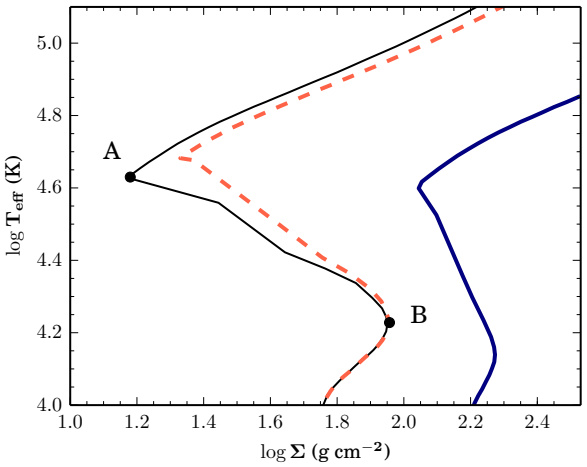

Fig. 8. An example of the surface density–effective temperature Σ-$T_{\rm eff}$ relations (S-curves) for an accretion disc around a $1.4\,\mathrm{M}_\odot$ neutron star at $R = 2\times10^4\,R_{\rm g}$ (solid black and red dashed curves) and $2\times10^5\,R_{\rm g}$ (thick blue curve). The black curve corresponds to $\alpha_{\rm cold} = 0.01$, $\alpha_{\rm hot} = 0.05$, the red dashed curve, to $\alpha_{\rm cold} = 0.01$, $\alpha_{\rm hot} = 0.03$, and the thick blue curve, to $\alpha_{\rm cold} = \alpha_{\rm hot} = 0.01$. For the black curve, the hydrogen ionisation instability begins in A and ends at B; analogous points can be determined for other curves.

Smak (1984) suggested the following simple scaling relations, assuming that the shape of the stability curve does not change and the critical points shift with the radius throughout the disc. Each of the critical points can be transformed by following formulae,

$$\log T'_{\rm eff} = \log T_{\rm eff} + a_r \log(R/2\times10^4 R_{\rm g}) + a_\alpha \log(\alpha/0.1), \tag{5}$$

$$\log \Sigma' = \log \Sigma + b_r \log(R/2\times10^4 R_{\rm g}) + b_\alpha \log(\alpha/0.1), \tag{6}$$

where $T_{\rm eff}$ and Σ are the effective temperature and surface density, respectively, numerically calculated at the reference point of $R = 2\times10^4 R_{\rm g}$ and $\alpha = 0.1$, where $R_{\rm g} \equiv GM/c^2$, and a and b are fitted coefficients. Then $T'_{\rm eff}$ and Σ' are transformed values of these quantites. In our procedure, we choose two pairs of values of R and α, for which we calculate the Σ-$T_{\rm eff}$ curves. We then calculate the positions of the points A and B, and then fit the coefficients a and b to the stability curves calculated at intermediate values. The resulting values are $a_r = -0.09$, $a_\alpha = -0.01$, $b_r = 1.11$, $b_\alpha = -0.73$.

In order to reproduce the observed amplitudes of dwarf novae outbursts, it was suggested that the viscosity parameter α must have different values on the upper and lower branches of stability curve (see, e.g., Lasota 2001, Done et al. 2007, for reviews). In our computations, we also assume it, implying $\Sigma_{\rm min} = \Sigma^{\rm A} \simeq \Sigma(\alpha_{\rm hot})$ and $\Sigma_{\rm max} = \Sigma^{\rm B} \simeq \Sigma(\alpha_{\rm cold})$. A bridging formula is used for the transition between the two values of α along the stability curve,

$$\log_{10}(\alpha) = \log_{10}(\alpha_{\rm cold}) + \frac{\log_{10}(\alpha_{\rm hot}/\alpha_{\rm cold})}{1 + (2.5\times10^4\,\mathrm{K}/T_{\rm c})^8}. \tag{7}$$

The above old, observationally motivated, approach, was confirmed by numerical simulations of the magneto-rotational instability (MRI, Balbus & Hawley 1991). This instability is supposedly the physical process that is acting behind the viscosity mechanism in astrophysical flows. The non-linear development of the MRI leads to the disc turbulence, and hence turbulent viscosity, because magnetic fields are frozen into the fluid in a differentially rotating disc. Thus, the MRI provides an efficient way to transport the angular momentum outwards in the disc and allow for accretion. It has been shown, e.g., in Janiuk et al. (2004), that the resistive diffusion of magnetic field, as quantified by the magnetic Reynolds number, is low in a cold state of the discs of stellar mass accreting compact objects (white dwarfs, neutron stars and black holes in binaries). Therefore, it is expected that the MRI turbulence disappears in the quiescent disc. In the outburst state, on the other hand, the action of MRI turbulence is efficient. Consequently, the approach postulated for these systems, namely the $\alpha_{\rm cold} < \alpha_{\rm hot}$ is justified, and we follow it here.

In our numerical approach, we first calculate the disc vertical structure as a sequence of local solutions. We then calculate the time-dependent radial structure, which yields the final light curve. This method is described in detail by Smak (1984) and Siemiginowska et al. (1996).

3.2. Results and discussion

Following Galloway et al. (2006), we assume $M_{\rm NS} = 1.4\,{\rm M}_{\odot}$, $R_{\rm NS} = 10\,{\rm km}$, and $D = 6.0\,{\rm kpc}$. We have estimated the average bolometric flux by scaling the ASM and BAT spectra to the Crab, adding them and then applying a correction for the emission beyond the energy ranges of those instruments of 50%. This yields $F_{\rm bol} \simeq 4.4\times10^{-9}$ erg cm^{-2} s^{-1}, and, assuming isotropy, $L_{\rm bol} = 4\pi D^2 F_{\rm bol} \simeq 1.9\times10^{37}$ erg s^{-1}. The accretion efficiency in the Newtonian approximation (e.g., Frank et al. 2002) is

$$\eta = \frac{GM_{\rm NS}}{R_{\rm NS}c^2} \simeq 0.21, \qquad (8)$$

which implies the accretion rate averaged over an outburst of

$$\dot{M} = \frac{L_{\rm bol}}{\eta c^2} \simeq 1.6\times10^{-9}\,{\rm M}_{\odot}\,{\rm yr}^{-1}. \qquad (9)$$

We assume $\dot{M} = 1.5\times10^{-9}\,{\rm M}_{\odot}\,{\rm yr}^{-1}$ in the calculations. We study models with $0.001 \le \alpha_{\rm cold} \le 0.1$ and with the ratio of $0.14 \le \alpha_{\rm cold}/\alpha_{\rm hot} \le 1.0$. We assume the disc outer radius equals $R_{\rm out} = 2\times10^5 R_{\rm g}$, which corresponds to about 80 per cent of the Roche-lobe radius of the neutron star. The disc inner radius is at $6R_{\rm g}$.

We have selected the time span from 20 January 2006 to 16 August 2006 for the ASM and the BAT light curves, and we summed the fluxes from them as shown in Fig. 7. This light curve shows relatively regular outbursts with high amplitude. As we found in Section 2, the quasi-period of this part of the data is $P \simeq 45\,{\rm d}$. We have calculated a large numbers of models, comparing them to the data.

The best agreement between the data and the calculated light curves (and for 300 grid points) was found for relatively low values of the viscosity parameters $\alpha_{\rm cold} = 0.01$ and $\alpha_{\rm hot} = 0.03$. This model, shown in Fig. 9, reproduces both the period and the approximate amplitude of outbursts. If we change the number of grid points, for the fixed values of the viscosity parameters, either to 500 or 150, the obtained light curves are only moderately affected, keeping the qualitative character of the variability.

The radial profiles of the surface density, Σ, are presented on the lower panel on Fig. 10. They are calculated at three different

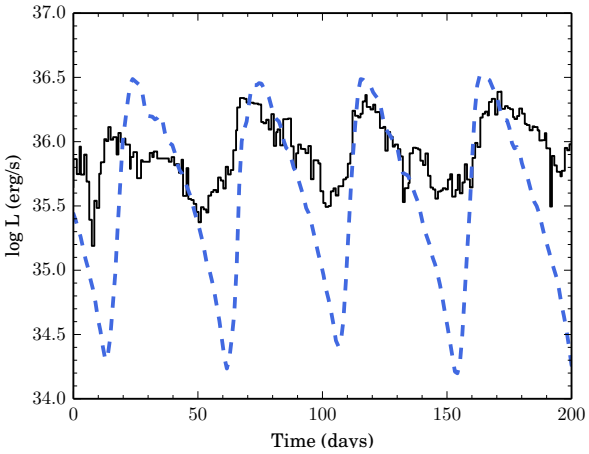

Fig. 9. The model for $\alpha_{\rm cold} = 0.01$, $\alpha_{\rm hot} = 0.03$ and the grid with $N = 300$. The solid curves show the observed light curve, given by the sum of one-day average ASM and BAT fluxes (the same as in Fig. 7), with the time of zero corresponding to MJD 53755. The dashed curves show the theoretical light curves.

stages of an outburst. The red solid, green dashed and blue dotted curves in the lower panel, marked by I, II, III, show the profiles of Σ at the onset, in the middle and at the peak of the outburst, which stages are shown by the red, green and blue filled cirles, respectively, in the upper panel.

The black and violet inclined straight lines correspond to the critical values of Σ at the cold and hot phase, respectively. The areas bound by those black and the violet lines define the unstable regions in the accretion disc at the cold and hot phase, respectively. We see that the surface density reaches the critical value (the onset of the instability) at $R > 10^4 R_{\rm g}$.

We find that the outburst amplitude decreases with the increasing $\alpha_{\rm cold}/\alpha_{\rm hot}$. Then, $\alpha_{\rm cold}$ determines the interval between outbursts and $\alpha_{\rm hot}$, the time scale of a single outburst. Both time scales decrease with the increasing value of α. We assume here the constancy of the average $\dot{M}$, which is justified by the constancy of the flux averaged over an outburst in the chosen data interval. However, changes of the $\dot{M}$ averaged on time scales longer than that of the outburst will lead to changes of the quasi-period and the amplitude of an individual outburst, as seen in the data. Specifically, for our chosen parameters, an increase of $\dot{M}$ above $1.5\times10^{-9}{\rm M}_{\odot}\,{\rm yr}^{-1}$ reduces the outburst amplitude and the duration of the minimum, while it increases the duration of the maximum. A decrease of $\dot{M}$ leads to the opposite behaviour. The instability disappears at $\dot{M} \gtrsim 5\times10^{-9}{\rm M}_{\odot}\,{\rm yr}^{-1}$. Thus, our model can explain the overall properties of the entire data set.

The different values of α in the cold and hot states that we found here to be necessary, are in general agreement with these suggested by observations of dwarf novae and soft X-ray transients. As it was found by Hirose et al. (2014), an intermittent thermal convection on the upper stable branch of the disc stability curve may strengthen the magnetic turbulence and significantly increase the value of α. Nevertheless, the values of α found here are relatively low, in the range of 0.01–0.03 for our best model. This means that the values of the Maxwell and Reynolds stresses in the cold and hot disc states are relatively similar, as it was also found in some shearing-box simulations (see King et al. 2007 and references therein). Thus, at least for the neutron star binary studied here, the poloidal magnetic field required to enhance the angular momentum transport in the

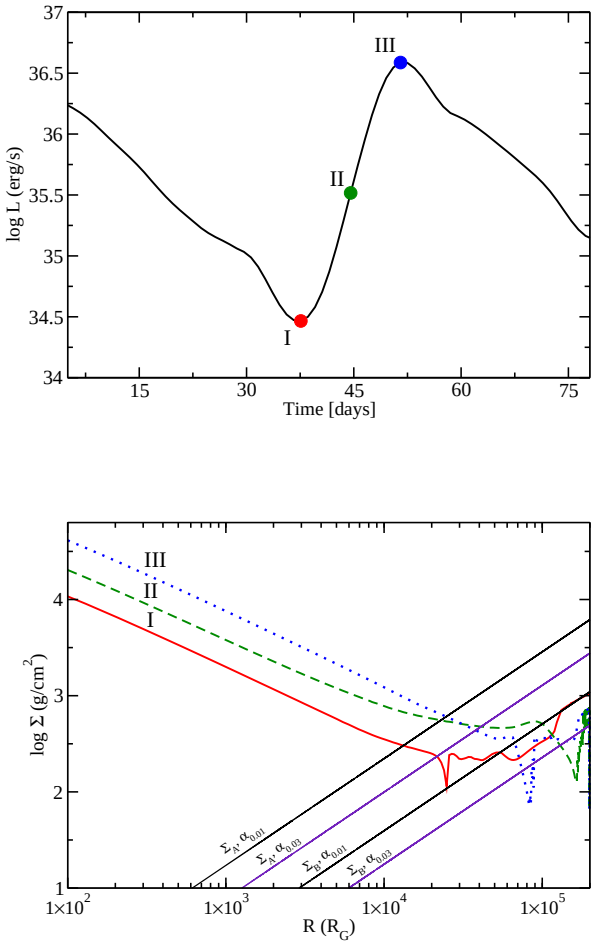

Fig. 10. The top panel: a part of the theoretical light curve calculated for $\alpha_{\rm cold} = 0.01$, $\alpha_{\rm hot} = 0.03$ and 300 grid points. The bottom panel: the corresponding radial profiles of the surface density, Σ (lower panel). The red solid line, green dashed line and blue dotted line correspond to three different stages shown as the red (I), green (II) and blue (III) filled circles on the light curve. The black and the violet straight lines in the lower panel correspond to the critical values of Σ as functions of the radius at the cold and a hot phase, respectively.

ionised disc cannot be very large, and the local MRI turbulence is sufficient to account for its behaviour. In particular, the results obtained here imply the value of β, the gas to magnetic pressure ratio, to be on the order of $\sim 1/(2\alpha)$ (Yuan & Narayan 2014), which corresponds to $\beta \sim$ 15–50. This gives tighter constraints than those resulting from other numerical simulations (see Yuan & Narayan 2014 for a review).

We note that Shih et al. (2005) proposed that the observed quasi-periodicity in 4U 1636–536 is explained by an instability due to the irradiation of the disc by X-rays. However, they did not perform any calculations to support their proposal. Our model does not invoke irradiation. We note that irradiation, due to the additional heating imposed on the disc by the X-rays, has a stabilizing effect. Therefore, it may still change the quantitative details of the disc instability model (Lasota 2015). As it was shown, e.g., by Dubus et al. (2001), somewhat longer decay-phase and recurrence times are obtained if irradiation is taken into account and the inner disc is allowed to be truncated between the outbursts. In our calculations, we do not take the disc truncation and irradiation into account.

There is a number of both observational and theoretical reasons justifying the neglect of irradiation in the case of 4U 1636–536. First, we have verified that the observed visual magnitude 17.5 mag of 4U 1636–536 (van Paradijs & McClintock 1994; Lyu et al. 2007) giving luminosity $L_{\rm vis} = 9 \times 10^{33}$ erg/s is consistent with the calculated visual luminosity of our model of non-irradiated accretion disc. In addition, we have checked that the observed visual luminosity of the source has been constant since 1990 (e.g. van Paradijs & McClintock (1994); Lyu et al. (2007)), but in contrast the average observed X-ray luminosity of 4U 1636–536 determined on the basis of RXTE light curve has substantially changed. Before 2000, X-ray luminosity was $\sim 2.3 \times 10^{37}$ erg/s but after 2000 it dropped to $\sim 1 \times 10^{37}$ erg/s. If the observed optical luminosity had been due to the reprocessing of X-rays in the 4U 1636–536, we would have observed a decrease in visual magnitude, but it was not the case. Furthermore, we have checked that the ratio of the average X-ray to optical luminosities, $L_X/L_{\rm vis}$, for 4U 1636–536 was $\sim$ 2500 before 2000 and $\sim$ 1100 after 2000. These values are high compared to other X-ray systems (Ritter & Kolb 2015).

Second, the standard division of X-ray binaries is for persistent and transient systems. 4U 1636–536 is persistent but its strong variability can be well explained by hydrogen instability, although the system never enters into quiescence. We have found, taking into account the mass transfer rate and the orbital period, that the system can be considered as transient or persistent depending on importance of the irradiation, as shown in fig. 1 of Coriat et al. (2012). On that figure, the $\dot{M}$ and period of 4U 1636–536 appear between the lines dividing transient (low $\dot{M}$) and persistent (high $\dot{M}$) systems either with (the lower line) and without (the upper line) irradiation. Since the source shows strong quasi-periodic oscillations, its position should be below the line dividing stable and unstable systems. This suggests that irradiation is not important in that system.

Third, the quiescent state is not achieved in 4U 1636–536, because the outbursts are too short for the disc to evacuate completely. This fact appears to be related to the lack of irradiation.

Fourth, we have found that the ratio of the irradiating to the viscous fluxes is less than the optical depth of the disc in a wide range of accretion rates for this system. Therefore, for ionized parts of the disc, the vertical and radial solutions can be obtained neglecting irradiation.

4U 1636–536 system can be a candidate for a separate class of SXTs in which irradiation could be neglected. Lack of irradiation leads to the shape of a light curve of 4U 1636–536 different from that of a soft X-ray transient, having similar rise and decay timescale, the small amplitude (comparing to classical SXT) of oscillations and no quiescence state.

4. Conclusions

We have analysed all the currently available X-ray data of LMXB 4U 1636–536 from the *RXTE*/ASM, *RXTE*/PCA, *Swift*/BAT and MAXI detectors, spanning together the energy range of 1.3–50 keV, and observing the source from 1996 to 2014. We have confirmed the previous finding of an appearance of the quasi-periodicity in the X-rays from the source in 2004 (Shih et al. 2005) and found it continued until 2006. The average period during that epoch is ≃45 d. However, the quasi-period drifts (increasing up to ∼70 d or decreasing up to ∼37 d) or disappears altogether, and its amplitude changes after 2006. The period of ≃45-d appears again during 2010–2011.

We then have considered a model of the hydrogen-ionisation disc instability. Using the formalism proposed by Smak (1984) to explain outbursts in cataclysmic variables, we have found that it can be successfully used for this accreting neutron-star. In order to reproduce a part of the X-ray light curve of 4U 1636–536 with a stable quasi-periodicity, we have numerically determined the vertical structure and calculated the radial time-dependent evolution of the accretion disc. We have estimated the average accretion rate based on the source distance, the X-ray light curve, and the accretion efficiency for the assumed mass and radius of the neutron star. The main free parameters of our model are then the values of the viscosity parameter, α.

We have found that, in order to reproduce the observed light curve given the source parameters, we need to use two different values of α for the cold (with mostly neutral hydrogen) and hot (with ionized hydrogen) phases, which confirms a number of previous findings, see, e.g., Lasota (2001), Done et al. (2007). Among the large number of the calculated models, the model with relatively low viscosity parameters, $\alpha_{\rm cold} = 0.01$, $\alpha_{\rm hot} = 0.03$ best reproduces both the amplitude and the period of the used part of the X-ray light curve.

Acknowledgements. We thank the anonymous referee for important comments, which have helped us to improve the paper. We would like to thank Bożena Czerny, Agata Różańska, Jean-Pierre Lasota-Hirszowicz, Galina Lipunova, Rupal Basak and Monika Mościbrodzka for helpful discussions. This work was partially supported by the POMOST/2012-6/11 Program of the Foundation for the Polish Science co-financed by the European Union within the European Regional Development Fund (MW and DGR), by the Polish National Science Centre grants 2015/17/N/ST9/01288 (MW), 2011/03/D/ST9/00656 (AS), 2012/05/E/ST9/03914 (AJ) and 2012/04/M/ST9/00780, 2013/10/M/ST9/00729 and 2015/18/A/ST9/00746 (AAZ). Calculations were performed on the PIRXGW computer cluster funded by the Foundation for Polish Science within the FOCUS program.

References

Alexander, D. R. 1975, ApJS, 29, 363
Alexander, D. R., Rypma, R. L., & Johnson, H. R. 1983, ApJ, 272, 773
Bagińska, P., Różańska, A., Janiuk, A., & Czerny, B. 2014, in XXXVI Polish Astronomical Society Meeting, p. 140
Balbus, S. A. & Hawley, J. F. 1991, ApJ, 376, 214
Bath, G. T. & Pringle, J. E. 1982, MNRAS, 199, 267
Belloni, T., Homan, J., Motta, S., Ratti, E., & Méndez, M. 2007, MNRAS, 379, 247
Bradt, H. V., Rothschild, R. E., & Swank, J. H. 1993, A&AS, 97, 355
Breedon, L. M., Turner, M. J. L., King, A. R., & Courvoisier, T. J.-L. 1986, MNRAS, 218, 487
Cannizzo, J. K., Ghosh, P., & Wheeler, J. C. 1982, ApJ, 260, L83
Casares, J., Cornelisse, R., Steeghs, D., et al. 2006, MNRAS, 373, 1235
Clarke, C. J. 1988, MNRAS, 235, 881
Coriat, M., Fender, R. P., & Dubus, G. 2012, MNRAS, 424, 1991
Cox, A. N. & Stewart, J. N. 1969, Nauchnye Informatsii, 15, 1
Cox, A. N. & Stewart, J. N. 1970, ApJS, 19, 243
Done, C., Gierliński, M., & Kubota, A. 2007, A&A Rev., 15, 1
Dubus, G., Hameury, J.-M., & Lasota, J.-P. 2001, A&A, 373, 251
Farrell, S. A., Barret, D., & Skinner, G. K. 2009, MNRAS, 393, 139
Faulkner, J., Lin, D. N. C., & Papaloizou, J. 1983, MNRAS, 205, 359
Frank, J., King, A., & Raine, D. J. 2002, Accretion Power in Astrophysics: Third Edition
Fujimoto, M. Y. & Taam, R. E. 1986, ApJ, 305, 246
Galloway, D. K., Psaltis, D., Muno, M. P., & Chakrabarty, D. 2006, ApJ, 639, 1033
Giles, A. B., Hill, K. M., Strohmayer, T. E., & Cummings, N. 2002, ApJ, 568, 279
Hasinger, G. & van der Klis, M. 1989, A&A, 225, 79
Hameury, J.-M., Menou, K., Dubus, G., et al. 1998, MNRAS, 298, 1048
Hirose, S., Blaes, O., Krolik, J. H., Coleman, M. S. B., & Sano, T. 2014, ApJ, 787, 1
Hoffman, J. A., Lewin, W. H. G., & Doty, J. 1977, ApJ, 217, L23
Ivezić, Ž., Connelly, A. J., VanderPlas, J. T., & Gray, A. 2014
Jahoda, K., Swank J. H., Giles A. B., et al. 1996, SPIE, 2808, 59
Janiuk, A., Czerny, B., Siemiginowska, A., & Szczerba, R. 2004, ApJ, 602, 595
Janiuk, A., Czerny, B. 2007, A&A, 466, 793
King, A. R., & Ritter, H. 1998, MNRAS, 293, L42
King, A. R., Pringle, J. E., West, R. G., & Livio, M. 2004, MNRAS, 348, 111
King, A. R., Pringle, J. E., & Livio, M. 2007, MNRAS, 376, 1740
Krimm, H. A., Holland, S. T., Corbet, R. H. D., et al. 2013, ApJS, 209, 14
Lasota, J.-P. 2001, New Astr. Rev., 45, 449
Lasota, J.-P. 2015, in Astrophysics of Black Holes – From fundamental aspects to latest developments, ed. C. Bambi, Springer, arXiv:1505.02172
Levine, A. M., Bradt, H., Cui, W., et al. 1996, ApJ, 469, L33
Lin, D. N. C. & Shields, G. A. 1986, ApJ, 305, 28
Lipunova, G. V. & Shakura, N. I. 2000, A&A, 356, 363
Lipunova, G. V. & Shakura, N. I., 2008, A&A, 485, 153
Liu, Q. Z., van Paradijs, J., & van den Heuvel, E. P. J. 2007, A&A, 469, 807
Markwardt, C. B., Tueller, J., Skinner, G. K., et al. 2005, ApJ, 633, L77
Matsuoka, M., Kawasaki, K., Ueno, S., et al. 2009, PASJ, 61, 999
Meyer, F. & Meyer-Hofmeister, E. 1982, A&A, 106, 34
Mineshige, S. & Shields, G. A. 1990, ApJ, 351, 47
Mineshige, S., Yamasaki, T., Ishizaka, C. 1993, PASJ, 45, 707
Ohashi, T., Inoue, H., Koyama, K., et al. 1982, ApJ, 258, 254
Paczyński, B. 1969, Acta Astron., 19, 1
Pringle, J. E. 1981, ARA&A, 19, 137
Ritter, H., & Kolb, U. 2015, Acta Polytechnica CTU proceedings, 2, 21
Różańska, A., Czerny, B., Życki, P. T., & Pojmański, G. 1999, MNRAS, 305, 481
Scargle, J. D. 1982, ApJ, 263, 835
Seaton, M. J., Yan, Y., Mihalas, D., & Pradhan, A. K. 1994, MNRAS, 266, 805
Shakura, N. I. & Sunyaev, R. A. 1973, A&A, 24, 337
Shih, I. C., Bird, A. J., Charles, P. A., Cornelisse, R., & Tiramani, D. 2005, MNRAS, 361, 602
Shih, I. C., Charles, P. A., & Cornelisse, R. 2011, MNRAS, 412, 120
Siemiginowska, A., Czerny, B., & Kostyunin, V. 1996, ApJ, 458, 491
Smak, J. 1982, Acta Astron., 32, 199
Smak, J. 1984, Acta Astron., 34, 161
Strohmayer, T. E. 1999, ApJ, 523, L51
Suleimanov V. F., Lipunova G. V., Shakura N. I., 2007, ARep, 51, 549
Suleimanov, V. F., Lipunova, G. V. & Shakura N. I. 2008, A&A, 491, 267
Tsunemi, H., Kitamoto, S., Okamura, S., & Roussel-Dupre, D. 1989, ApJ, 337, L81
van Paradijs, J., van der Klis, M., van Amerongen, S., et al. 1990, A&A, 234, 181
van Paradijs, J., McClintock, J. E., 1994, A&A, 290
VanderPlas, J., Connolly, A. J., Ivezic, Z., & Gray, A. 2012, in Proceedings of Conference on Intelligent Data Understanding (CIDU), p. 47
Willmore, A. P., Mason, K. O., Sanford, P. W., et al. 1974, MNRAS, 169, 7
Yuan, F. & Narayan, R. 2014, ARA&A, 52, 529
Zhang, W., Lapidus, I., White, N. E., & Titarchuk, L. 1996, ApJ, 473, L135